Iraqi Journal of Physics, 2025 *Vol. 23, No.3, PP.40-49*
https://doi.org/10.30723/ijp.v23i3.1416 *P-ISSN: 2070-4003*
E-ISSN: 2664-5548

Structural, Electronic, and Optical Properties of HgSe Monolayer: Density Functional Theory Calculations

Aqeel M. Ali[1*] and Mohanned J. Mohammed[2]
[1]*Department of Material Science, Polymer Research Center, University of Basrah, Basrah, Iraq*
[2]*Department of Physics, College of Science, University of Basrah, Basrah, Iraq*
[*]Corresponding author: aqeel.mohsin@uobasrah.edu.iq

Abstract
To investigate the structural, electrical, and optical properties of a single layer of two-dimensional mercury selenide (HgSe), density functional theory is used for the analysis of the material. To ensure the monolayer's structural and thermal stability, it is of the utmost importance to ascertain the phonon frequency. Computer simulations based on first principles were used in order to investigate the structural lattice parameter, which is in good agreement with experimental results. The two-dimensional HgSe is dynamically stable according to the positive phonon frequencies. The 2D-HgSe has the semiconductor characteristic of a direct band gap of about 1.731 eV, located at the Γ point. The static dielectric constant is 1.34 for a semiconductor characteristic. The HgSe monolayer is a transparent material with a static refractive index of 1.16, besides an anti-reflective characteristic. The refractive index had a lowest value of 0.76 at high energy. 2D-HgSe has a UV optical absorption characteristic.

Article Info.

Keywords:
DFT, HgSe Monolayer, 2D Materials, Phonon Spectra, Optical Properties.

Article history:
Received: Jan.04, 2024
Revised: Mar. 17, 2025
Accepted:Apr. 07, 2025
Published:Sep. 01,2025

1. Introduction
Topological insulators (TIs) have raised a plentiful attentiveness from researchers because of their splendid characteristics and their uses in quantum computing and spintronics [1]. Due to the flexibility of opened edge states from particles-reflection, two-dimensional (2D) TIs are thought to be more promising items than bulk TIs for spin conveyance implementations [2-8]. However, because the tiny band gaps, the quantum spin Hall leverage of current two-dimensional topological insulators only take places under super cold conditions [9]. For both basic and practical reasons, the hunt for two-dimensional topological insulators with insulators has thus accelerated recently [10-14]. 2D substances have garnered a plentiful attentiveness since the discovery of graphene because of its many uses in solar cells, optoelectronics, and spintronics [15]. Single-layer separation by mechanical or chemical exfoliation is made easier by the fact that the majority of 2D materials have 3D layered parent equivalents that show weak out-of-plane Van der Waals interactions and strong in-plane covalent bonding [16-18]. Additionally, a variety of materials with firm two-dimensional frames and a broad domain of intriguing features exist outside of 3D layered materials. It is interesting to note that numerous elements and compounds have a 2D honeycomb structure that is fixed in a flat or buckled shapes, according to recent theoretical simulations [19-21]. Therefore, these materials' honeycomb lattice provides a special environment for the hunt for new quantum spin Hall (QSH) insulators with wide band gaps. One of the special characteristics of the semimetal 3D mercury selenide (HgSe) with space group F43m is that its band skeleton shows an inversion of the Γ6 and Γ8 band ordering [22, 23]. Since of its semimetallic character, HgSe is also anticipated to have Dirac-electronic levels, which are challenging to measure since they are constantly connected to metallic bulk states [24].

Nevertheless, the systems become 3D TIs under stress that creates a gap between the highest valance bands. HgSe is a two-dimensional hexagonal lattice of mercury and selenide atoms, similar to graphene, which has sparked interest in the field of quantum computing and nanoelectronics due to its potential applications [25]. In the current work, we make a prediction based on density functional theory (DFT) computations that a two-dimensional monolayer of HgSe with a buckled honeycomb topology is stable.

2. Methodology

The optoelectronic properties of the Hg and HgSe ML were investigated through CASTEP program with the use of DFT [26]. Norm-conserving, pseudopotential, and Perdew–Burke–Ernzerhof (PBE) exchange energy and Hartree–Fock exchange energy were employed, along with the full PBE correlation energy (PBE0 hybrid-functional) analysis to investigate the exchange interaction and correlation [27, 28]. The unit cell of a HgSe ML was created from the planar (1 1 1) surface of the bulk zincblende HgSe crystal (cubic 216-$\bar{F}$43m space group). A vacuum thickness was assumed in order to prevent interlayer connection with the super-cell's length of 15 A, and the monolayer set corresponding to the a-b plane and normal direct c was used for all calculations. The force tolerance was 0.01 eV/Å to optimize the structure using the Broyden-Fletcher-Goldfarb-Shanno (BFGS) algorithm. An energy of 20 meV for confinement and 500 eV mesh for cut-off were utilized in our Plane Wave foundation sets. To incorporate the Brillouin zone in two dimensions, a Monkhorst-Pack k-point grid measuring 21×21×1 was used. It was determined that a supercell method was used to compute the phonon spectra [29]. The optical properties, electrical band structure, and partial density of states were all investigated within the same theoretical framework. Fig.1 illustrates the honeycomb structure of 2D-HgSe monolayer.

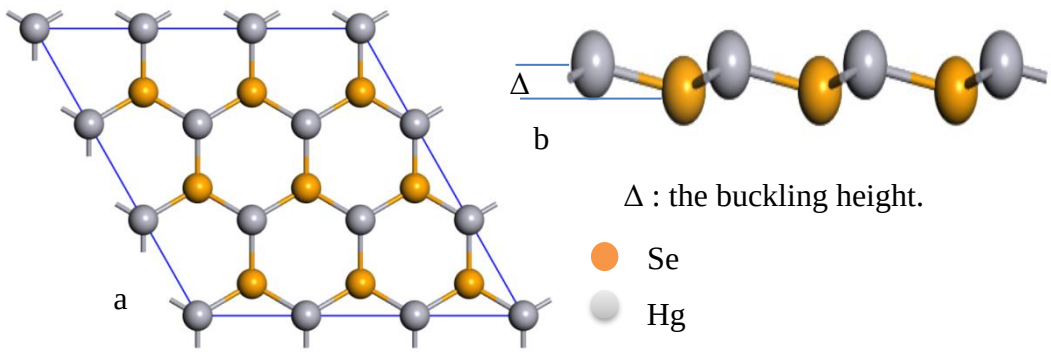

Figure 1: The structure of 2D-HgSe monolayer. a) front view and b) side view.

3. Results and Discussion

Fig.1 shows that pure HgSe ML has a hexagonal shape. In contrast to the planar structure of graphene, the low-buckled arrangement of HgSe ML is characterized by the segregation of Hg and Se atoms into separate sublattices. Consistent with earlier findings, the lattice constant and Hg-Se bond length in HgSe ML are 4.257 and 2.499 Å, respectively, during structural relaxations [30, 31]. Additionally, the buckling height between the Hg and Se plane in the z-direction is $\Delta = 0.45$ Å.

The band structure was determined by solving the Kohn–Sham equation for various k-points along the high-symmetry wave path. The electronic band structure of bulk HgSe is distinctive and essential for comprehending the electrical and optical properties of a material. In solid-state materials, atoms are densely packed, resulting in

reduced interatomic separation distances. This proximity causes the outer orbitals to overlap and interact significantly, leading to the formation of electronic bands. The band structure, seen in Fig. 2, was computed using the energy-optimized lattice parameter of 6.22 Å (the experimental value is 6.08 Å [30]). The CASTEP algorithm automatically establishes the Fermi energy at zero, as denoted by the dotted horizontal line on the band structure diagram. Figure 2 illustrates the electronic band structure of zinc blende HgSe at the computed equilibrium lattice constant along the high symmetry k-path within the first Brillouin zone of its primitive cell. The computation was executed throughout the energy spectrum of -8 to +10 eV. The band structure calculation figure indicates that the HgSe crystal possesses a direct semiconductor characteristic at the high symmetry G-point, measuring 0.435 eV, which is in high accuracy to the absorption onset of 0.42 eV [30]. This finding corroborates prior research indicating that mercury selenide functions as a strict gap semiconductor [30].

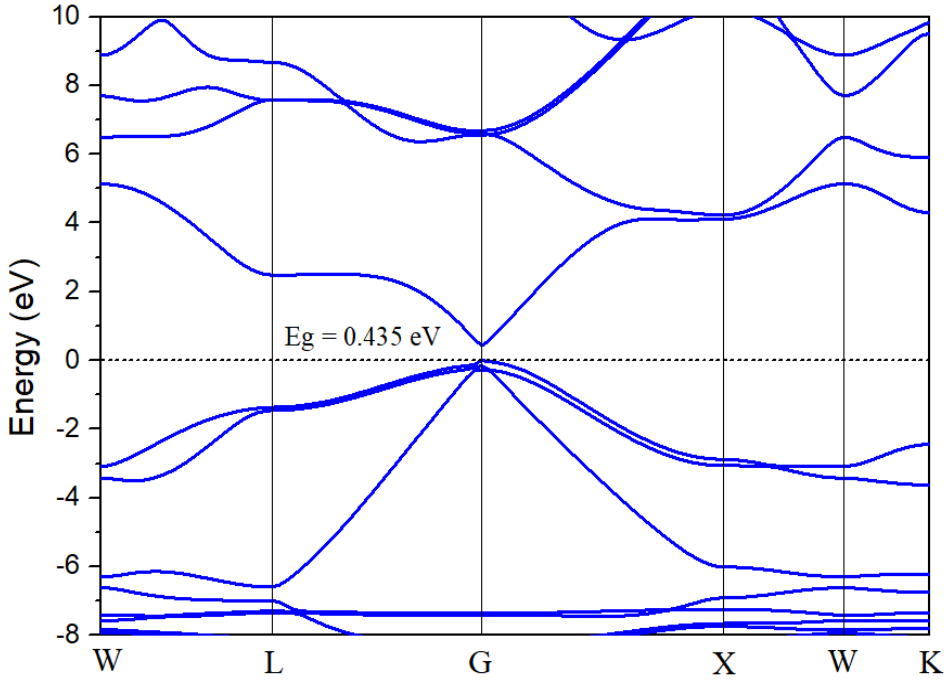

Figure 2: Electronic band structure for bulk HgSe.

For the 7×7×1 super cell HgSe ML, the phonon dispersion curve is shown in Fig.3. The fact that the HgSe monolayer has only positive phonon frequencies in the initial Brillouin zone indicates that it is a dynamically stable structure. According to Fig.2, the unit cell's two atoms generate six optical modes and three acoustic modes. Three separate acoustic modes are present: the longitudinal (LA) mode that corresponds to compressional waves, the transverse (TA) mode that corresponds to shear waves, and the out-of-plane atomic displacement-corresponding acoustic, z-axis acoustic mode (ZA).

Fig.4 illustrates the band structure of HgSe monolayer calculated using PBE0, revealing that HgSe possesses semiconductor characteristics with a direct band gap of 1.731 eV. The conduction band minimum (CBM) and the valence band maximum (VBM) are situated at the G point, consistent with prior DFT results [30,31]. By mapping these bands onto several atomic orbitals, it ascertains that the bands proximate to the Fermi level at the G point predominantly originate from one s-state and two p-states, which conform to the conventional band order, so indicating that the perceived band inversion is authentic.

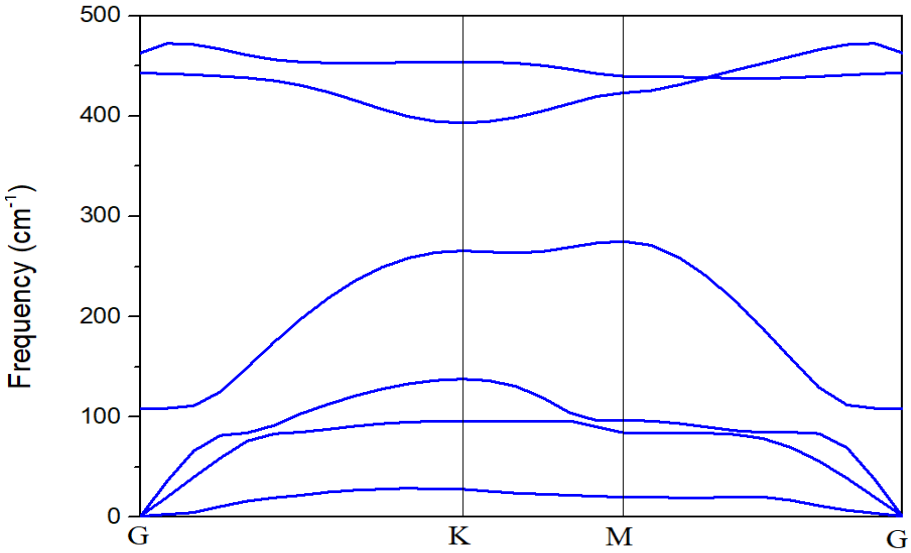

Figure 3: Phonon dispersion curve for HgSe ML.

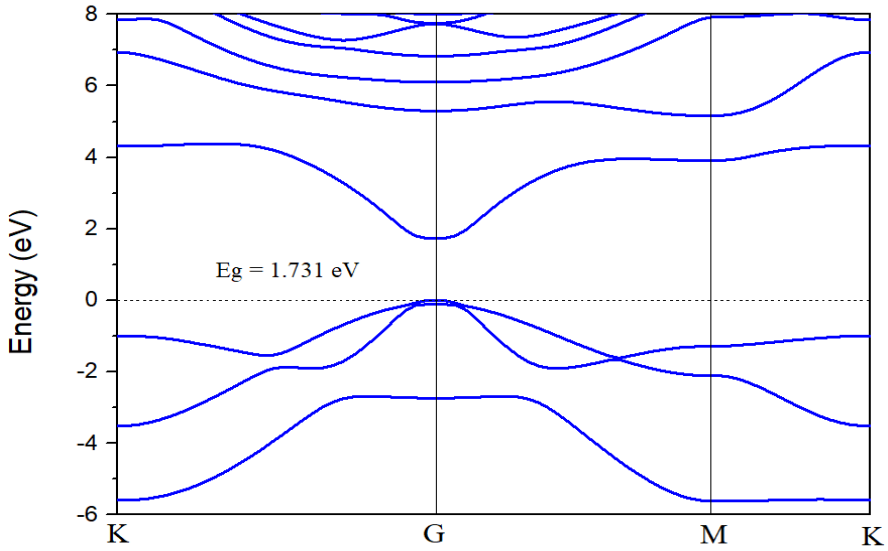

Figure 4: Electronic band structure for HgSe

In order to examine the spin-dependent electrical characteristics of HgSe monolayer, calculations on the Projected Density of States (PDOS) were conducted, as seen in Fig.5. It was discovered that the HgSe ML is a semiconductor, with a greater number of possible states at the fermi level. The semiconductor kernel of HgSe monolayer is attributed to the of the Se *p*-orbital and the Hg *s*-orbital as shown in Fig.5, which is separated around the Fermi level. The PDOSs calculated for Hg and Se demonstrated a dominant role in relation to the Fermi energy (E_F). Nevertheless, these states are somewhat more extensive in energy (ranging from -3 eV to 0.5 eV), and they are extended together in the energy range. These states disclose the covalent character of the investigated materials as a result of the significant hybridization that occurs between the cation and anion atoms. In this study, it was shown that the electronic band structures of HgSe single-layer were solely derived from Hg and Se around the E_F. The PDOS for Se states had a maximum value of around -0.41 eV downward for E_F. With the exception of a small tail seen around E_F up to 0.3 eV, DOS displayed a gradual decreasing. The

electronic states subsequent to this energy range are attributed to selenium with a little contribution from mercury.

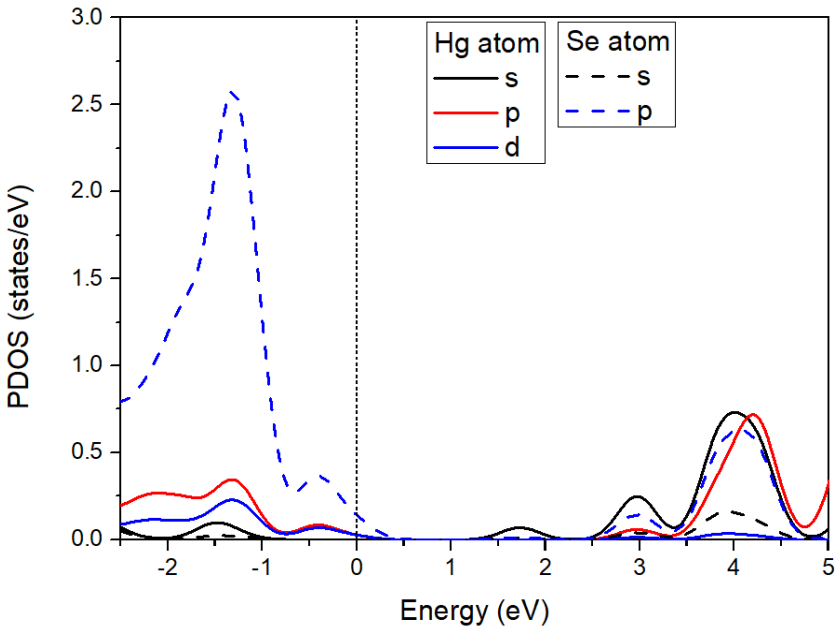

Figure 5: Electron partial density of states of HgSe

The examination of optical characteristics could be portrayed by assessing the interaction between light wave and a mater, focusing on the basic parameter, the dielectric function. The essential element pertains to the negative charge carrier configurations of a solid and their permission in optical spectroscopic datum. The dielectric function is consistent from two principal components: the first one is real component and the second is imaginary component. The equation $\varepsilon = \varepsilon' + i\varepsilon''$ characterizes the electronic-radiation spectral response of a material. Analyzing the spectral lineaments of the two components of ε enables the evaluation of the computational properties of many optical spectra, including the optical absorption coefficient, reflectivity, refractive index and conductivity.

The dielectric function for the electric field vector that is polarized in a direction parallel to the c-axis of the crystallographic structure was calculated and shown in Fig.6. The spectra of ε' in Fig.6 show high values at 1.50 and 7.98 eV, which thereafter descends to a first critical point $\varepsilon'=1.34$ at 0.00 eV. These results once again demonstrate the inherent wide direct band gap characteristic of the semiconductor HgSe monolayer, as previously mentioned in band structure and PDOS shown in Figs. 5. The first critical point of $\varepsilon''(\omega)$ is 5.6 eV, approximate to the computed semiconductor band gap value and often referred to as the fundamental absorption edge. This observation validates the occurrence of the interband transitions from the Γ point. The spectra of $\varepsilon''(\omega)$ exhibited a conspicuous and substantial peak at 9.35 and 10.79 eV.

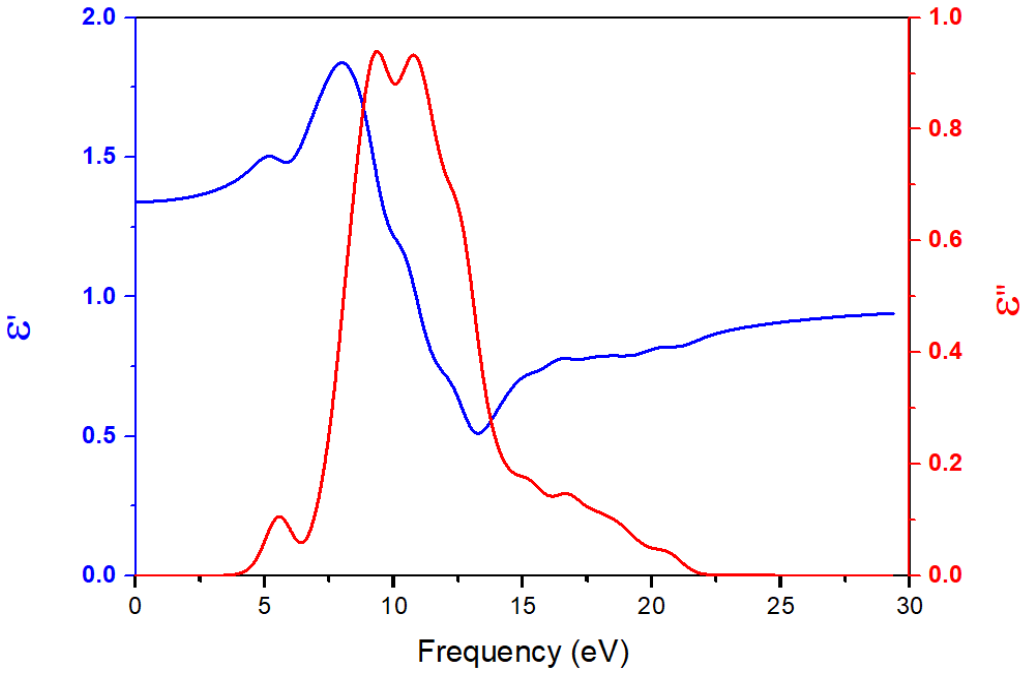

Figure 6: Dielectric function, real ε′(ω) and imaginary ε′′(ω) parts of HgSe.

The HgSe monolayer sheet and its extinction coefficient are depicted in Fig.7. The extent of light bending or refraction upon interaction with the substance is denoted by the refractive index n(ω). The HgSe monolayer possesses a static refractive index of 1.16. The refractive index exhibited a nonlinear behavior, gradually increasing and attaining its initial maximum at 5.17 and 8.10 eV. The refractive index had a lowest value of 0.76 at 13.49 eV. It appears to stabilize in the ultraviolet range following several oscillations. The influence of oscillation amplitude on the electric field of the incident electromagnetic wave is associated with the extinction coefficient K(ω). The extinction coefficient K(ω) is depicted in Fig.7. The peak values in the extinction coefficient K(ω) spectra were 0.04 and 0.43 at 5.6 and 11.08 eV, respectively. At this particular energy level, the material absorbed photons swiftly.

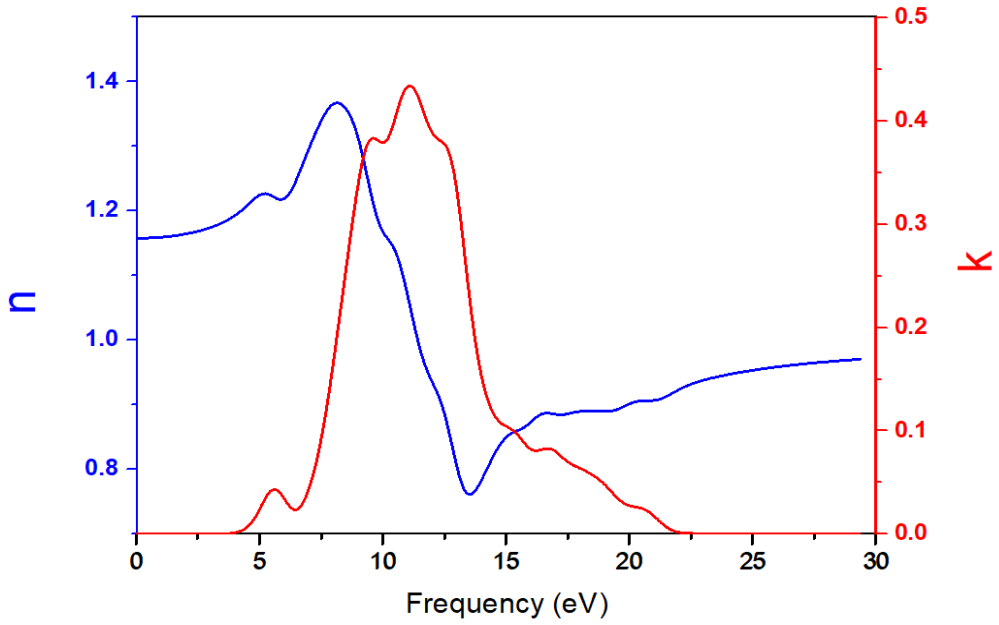

Figure 7: Refractive index n(ω) and extinction coefficient k(ω) parts of HgSe ML.

Reflectivity is a fundamental concept that is connected to the optical properties of solids. This concept is associated with the optical properties of solids. To examine the linear optical behavior that occurred during this research, the transitions in normal incident reflectivity between the valence bands and the downward conduction bands were investigated. An illustration of the features of reflectivity that can be observed in the optical spectrum can be found in Fig.8. These elements are displayed within the photon energy domain, which spans from 0 to 30 eV. According to the findings presented in Fig.8, the monolayer HgSe revealed a reflectivity lower than 5% when exposed to electromagnetic radiation with a photon energy greater than 15 eV. The static value of the reflectivity (R(0)) for the monolayer was 0.5% when the photon energy was equal to 0 eV. One possible interpretation of this finding is that monolayer HgSe possesses anti-reflective characteristics. At photon energies of 9.2, 11.2, and 12.9 eV, the single-layer HgSe was seen to have a maximum reflectivity of around 0.39%, 0.43%, and 0.45%, respectively. Over the whole spectrum of infrared and visible-ultraviolet light, which extends from zero to 15.0 eV, a significant reflectance was found to be present. Within the spectrum of ultraviolet-electromagnetic radiation, which runs from 8 to 15 electron volts, it was demonstrated that the medium of maximum reflectivity did exist. In addition, the monolayer system demonstrated a lowered reflectivity across the range of 16 to 30 eV, which clearly demonstrates the usefulness of the system. On the energy spectrum, the significant reflection observed for energy levels lower than 2.5 eV demonstrated the characteristic of robust conductivity within the lower energy bandwidth. This was observed for energy levels that were lower than 2.5 eV.

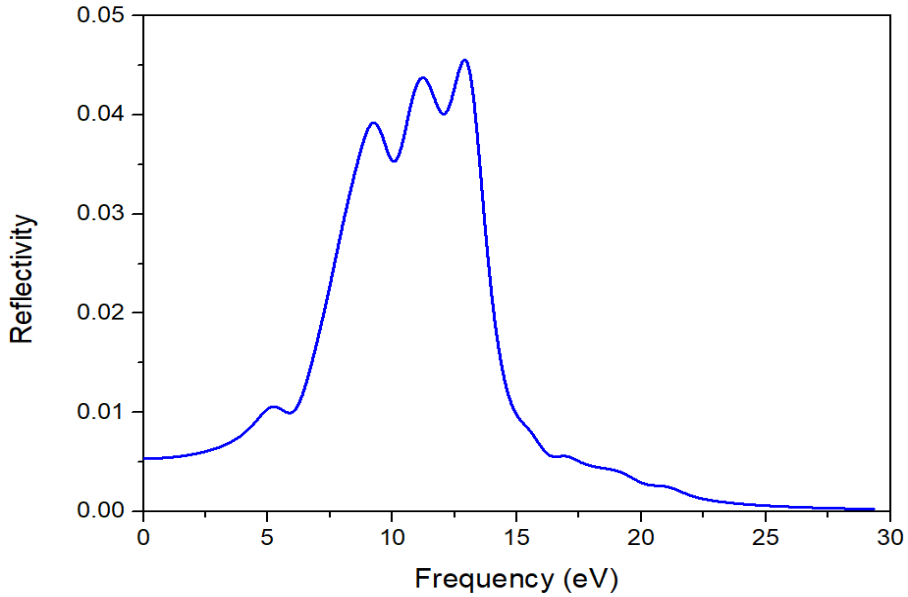

Figure 8: Reflectivity of HgSe ML.

The investigation of the absorption coefficient spectrum, which provides a more comprehensive degree of knowledge, may provide a better understanding of the electrical structural features of the two-dimensional materials that are the subject of the current research. One of the most important parameters for evaluating optical qualities in optoelectronic applications is the frequency-dependent absorption coefficient, shown in Fig. 9. This coefficient is determined for two different electric field directions. During the process of electromagnetic wave propagation through a medium, the light absorption coefficient is the proportion of light intensity that is attenuated per unit distance. A direct relationship exists between the imaginary component of the dielectric function and the extinction coefficient, as seen in Fig. 7. This relationship is directly related to the

absorption coefficient. A material's absorption coefficient is a measure used to determine the depth to which light can penetrate the material. A decrease in the amount of light absorbed by the material leads to a decrease in the substance's absorption coefficient. 4.7 eV is the energy at which the initial of first absorption peak was observed to be occurring. The largest absorption peak may be found within the ultraviolet (UV) area, which corresponds to an energy of 11.3 eV. The fact that monolayer HgSe exhibited a considerable value of absorption at 7.9×10^4 cm^{-1} indicates that it can hold prospective applications as a UV absorber. In the low energy range of 4 eV, the absorption coefficient was so low that it is practically nonexistent.

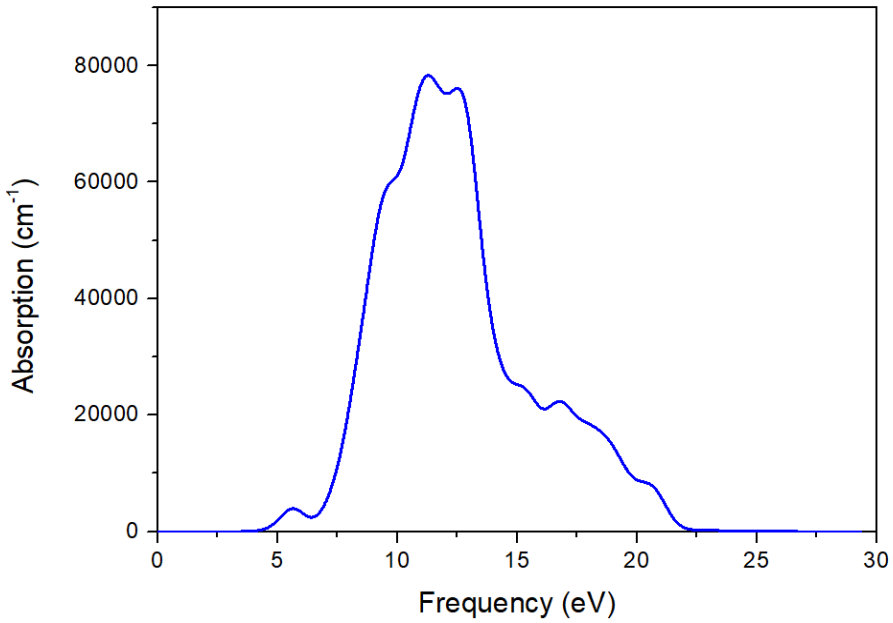

Figure 9: Absorption of HgSe ML.

4. Conclusions

The Plane Wave (PW) basis set method of DFT was used to study the electrical and optical properties of the HgSe monolayer on its own. The computed PDOS plots have demonstrated that the Hg 4p and Se 4p orbitals are primarily responsible for the partition of the states about the Fermi energy. When the pure HgSe monolayer was subjected to high photon energy, it was demonstrated through the examination of optical spectrum functions that the absorption of the monolayer was, on average, not very significant. The refractive index presented the HgSe monolayer as a transparent material. The reflectivity was very weak in the UV/Vis range, and the material was transparent. The real part of the dielectric function has oscillation around the standard space value.

Acknowledgements

The authors would like to thanks thank the University of Basrah, Polymer Research Centre, Department of Material Science for their assistance in carrying out this work.

Conflict of Interest

Authors declare that they have no conflict of interest.

References

1. N. Shukla and G. A. Ahmed, Mater. Today: Proce., **45**, 4819 (2021). https://10.1016/j.matpr.2021.01.293.

2. Y. Yin, Y. Gao, L. Zhang, Y. Zhang, and S. Du, Sci. China Mater., **67**, 1202 (2024). https://10.1007/s40843-023-2846-5.
3. T. Olsen, E. Andersen, T. Okugawa, D. Torelli, T. Deilmann, and K. S. Thygesen, Phys. Rev. Materials, **3**, 024005 (2019). https://10.1103/PhysRevMaterials.3.024005.
4. A. Bafekry, M. Faraji, S. Hasan Khan, M. M. Fadlallah, H. R. Jappor, B. Shokri, M. Ghergherehchi, and G. S. Chang, Scientific Reports., **14**, 12695 (2024). https://10.1038/s41598-024-63580-0.
5. A. Bafekry, S. Karabsizadeh, M. Faraji, H. R. Jappor, A. A. Ziabari, M. M. Fadlallah, M. Ghergherehchi, and G. S. Chang, Adv. Theo. Simulation., **7**, 2400438 (2024). https://10.1002/adts202400438.
6. A. Bafekry, M. M. Fadlallah, M. Faraji, S. Hasan Khan, H. R. Jappor, B. Shokri, M. Ghergherehchi, and G. S. Chang, Phys. Chem. Chem. Phys., **26**, 11056 (2024). https://10.1039/D3CP05360A.
7. A. Bafekry, B. Mortazavi, M. Faraji, M. Shahrokhi, A. Shafique, H. R. Jappor, C. Nguyen, M. Ghergherehchi, and S. A. H. Feghhi, Scientific Reports., **11**, 10366 (2021). https://10.1038/s41598-021-89944-4.
8. H. R. Jappor, A. O. M. Almayyali, H. A. Mezher, S. Al-Qaisi, S. Bin-Omran, and R Khenata, Surf. Interfaces, **54**, 105261 (2024). https://10.1016/j.surfin-2024-105261.
9. R. Meng, L. M. C. Pereira, J. V. Vondel, J. W. Seo, J. Locquet, and M. Houssa, ACS Omega., **9**, 31890 (2024). https://10.1021/acsomega.4c03502.
10. K. S. Novoselov, A. K. Geim, S. V. Morozov, D. jiang, Y. Zhang, S. V. Dubonos, I. V. Grigorieva, and A. A. Firsov., Science, **306** (2004). https://10.1126/science.1102896.
11. K. S. Novoselov, A. K. Geim, S. V. Morozov, D. Jiang, M. I. Katsnelson, I. V. Grigorieva, S. V. Dubonos, and A. A. Firsov, Nature, **438** (2005). https://10.1038/nature04233.
12. A. M. Ali, Iraqi J. Sci., **62**, 12 (2021). https://10.24996/ijs.2021.62.12.9.
13. K. Ashutosh, A. Devi, A. Kumar, A. Singh, and R. Adhikari, AIP Conf. Proc., **2995**, 020104 (2024). https://10.1063/5.017796.
14. A. M. Ali, Iraqi J. Sci., **64**, 1 (2023). https://10.24996/ijs.2023.64.1.20.
15. A. H. Castro Neto, F. Guinea, N. M. R. Peres, K. S. Novoselov, and A. K Geim, Rev. Mod. Phys., **81** (2009). https://10.1103/RevModPhys.81.109.
16. A. M. Ali, J. Kufa-Phys., **11**, 2 (2019). https://10.31257/JKP/2019/110209.
17. T. Vishal, K. Narender, B. K. Rao, M. L. Verma, H. D. Sahu; V. Swati, and C. Anil Kumar, Phys. E: Low-dimen. Syst. Nanostruc., **133** (2021). https://10.1016/j.physe.2021.114812.
18. B. Chettri, P. K. Patra, M. Lalmuanchhana, S. Verma, B. K. Rao,M. L. Verma, V. Thakur, N. Kumar, N.N. Hieu, and D.P. Rai, Inter. J. Quan. Chem., (2021). https://10.1002/qua.26680.
19. N. H. Malik, Q. Rafiq, M. F. Nasir, S. Azam, M. T. Khan, G. A. M. Mersal, and M. M. Hessien, Inter. J. Quan. Chem., (2024). https://10.1002/qua.27486.
20. S. K. Matta, C. Tang, A. P. OMullane, A. Du, and S. P. Russo, ACS App. Nano Mater. **5**, 10 (2022). https://10.1021/acsanm.2c02812.
21. K. R. Abidi and P. Koskinen, Phys. Rev. Mater., **6**, 124004 (2022). https://10.1103/PhysRevMaterials.6.124004.
22. N. Habibes, A. Boukortt, S. Meskine, A. Benbedra, Y. Mamouni, and H. Bennacer, J. Sol. State Sci. Tech., **13**, 013013 (2024). DOI:10.11492162-8777/ad1f8f.
23. G. Korotcenkov, *Hg-based narrow bandgap II-VI semiconductors Handbook of II-VI Semiconductor-Based Sensors and Radiation Detectors*, (Springer, Cham.,2023). https://10.1007/978-3-031-20510-1.
24. M. Debbarma, B. Debnath, D. Ghosh, S. Chanda, R. Bhattacharjee, and S. Chattopadhyaya, J. Phys. Chem. Sol., **131**, 86 (2019). https://10.1016/j.jpcs.2019.03.009.
25. J. Li, C. He, L. Meng, H. Xiao, C. Tang, X. Wei, J. Kim, N. Kioussis, G. M. Stocks, and J. Zhong, Nature: Sci. Rep., **5**, 14115 (2015). https://10.1016/j.jpcs.2019.03.009.
26. S. J. Clark, M. D. Segall, C. J. Pickard, P. J. Hasnip, M. I. J. Probert, K. Refson, and M. C. Payne, "First principles methods using CASTEP," *Zeitschrift für kristallographie-crystalline materials*, **220** 5-6 (2005). https://10.1524/zkri.220.5.567.65075.
27. J. P. Perdew, A. Ruzsinszky, G. I. Csonka, O. A. Vydrov, G. E. Scuseria, L.A. Constantin, X. Zhou, and K. Burke, Phys. Rev. let., **100**, 136406 (2008). https://10.1103/PhysRevLett.100.136406.
28. S. Smiga and L. A. Constantin, The J. Phys. Chem., A **124**, 27 (2020). https://10.1021/acs.jpca.0c04156.
29. H. Şahin, S. Cahangirov, M. Topsakal, E. Bekaroglu, E. Akturk, R. T. Senger, and S. Ciraci, Phis. Rev., B **80**, 155453 (2009). https://10.1103/PhysRevB.80.155453.
30. K. U. Gawlik, L. Kipp, and M. Skibowski, Phys. Rev. Lett., **78**, 16 (1997). https://10.1103/PhysRevLett.78.3165.
31. S. Li, W. Ji, C. Zhang, P. Li, and P. Wang, J. Mater. Chem., C **4** (2016). https://10.1039/c6tc00020g.

دراسة سيانيد الزئبق أحادي الطبقة بأستعمال نظرية دالة الكثافة

عقيل محسن علي[1] ومهند جاسم محمد[2]
[1] قسم علوم المواد، مركز أبحاث البوليمر، جامعة البصره، البصره، العراق
[2] قسم الفيزياء، كلية العلوم، جامعة البصره، البصره، العراق

الخلاصة
أجريت هذه الدراسة باستعمال نظرية دالة الكثافة للتحقق من أهم المواصفات التركيبية والخصائص الالكترونية والسلوك الضوئية لمادة سيلينايد الزئبق المصممة بشكل ثنائي الابعاد وذات طبقة أحادية. لغرض التحقق من ألاستقرار و الثباتية الحرارية لتركيب سيلينايد الزئبق أحادي الطبقة فأن من الجدير بألاهتمام هو تحديد طيف ترددات الاهتزاز الحراري. بألاعتماد على المبادئ ألاساسية أستعملت المحاكاة الحاسوبية للتحقق من الخصائص ألكهربائية والضوئية لطبقة أحادية جرى تصميمها من مادة سيلينايد الزئبق. في مجال مواد الالكترونيات النانوية يتبين ان الخصائص الاصيلة الداخلية لشريحة أحادية الطبقة من سيلينايد الزئبق جعلتها مناسبة بشكل أستثنائي لمواد ثنائية الابعاد. طبقا للتعرف على الخصائص الذاتية لاحادية الطبقة لذلك فأن أستكشافها يمهد لتحقيق هدفها. يضاف الى ذلك أن الخصائص الضوئية لسيلينايد الزئبق أحادي الطبقة تم دراستها والتحقق من أمكانية تطبيقها في مجال تطبيقات ثنائية ألابعاد. ألخصائص الضوئية التي هي على قدر كبير من ألاهمية في هذه الدراسة كانت معامل ألامتصاص الضوئي والانعكاسية ودالة فقدان الطاقة.

الكلمات المفتاحيه: نظرية دالة الكثافة، مادة ثنائية ألابعاد، سيلينايد الزئبق أحادي الطبقة، طيف ألاهتزاز، الخصائص الضوئية.